SUPPORTING INFORMATION FILE

FOR

Electrochemical CO_2 conversion technologies: state-of-the-art and future perspective

Remko J. Detz,[*a] Claire J. Ferchaud,[b] Arie J. Kalkman,[c] Jasmin Kemper,[d] Carlos Sánchez Martínez,[c] Marija Saric,[b] and Manoj V. Shinde[b]

* Correspondence: remko.detz@tno.nl

[a] Energy Transition Studies (ETS), Netherlands Organization for Applied Scientific Research (TNO), Radarweg 60, 1043 NT Amsterdam, The Netherlands.

[b] Sustainable Technologies for Industrial Processes (STIP), Netherlands Organization for Applied Scientific Research (TNO), P.O. Box 1, 1755 ZG Petten, The Netherlands.

[c] Sustainable Process and Energy Systems (SPES), Netherlands Organization for Applied Scientific Research (TNO), P.O. Box 6012, 2600 JA Delft, The Netherlands.

[d] IEA Greenhouse Gas R&D Programme, Pure Offices, Cheltenham Office Park, Hatherley Lane, Cheltenham, GLOS, GL51 6SH, United Kingdom

Electrochemistry may appear an attractive approach to convert a stable molecule like CO_2 into an array of carbon-based products, such as carbon monoxide (CO), formic acid (CHOOH), and ethylene (C_2H_4). Here we describe the methodology to investigate six routes to electrochemically convert CO_2 to produce CO (2 routes), syngas (1 route), formic acid (1 route), and ethylene (2 routes). The two key technologies we investigate for these routes, i.e. low temperature electrolysis and high temperature electrolysis, are at a relatively low development level and we use future developments and learning curves to project the costs of our six routes up to 2050.

In this supporting information file, we present the methodology behind the techno-economic evaluation of the six electrochemical CO_2 conversion routes. Some supplementary information about the state-of-the-art of the different routes is added in several tables and figures. In the third chapter, the sensitivity analysis of the four routes are presented that are not discussed in the main paper.

Contents

1 Methodology

For each of the routes we determine the technical status of the involved technology in terms of system size and configuration, technology readiness level (TRL), energy and mass balances, current investment costs, and cumulative installed capacity.

1.1 System size and configuration

Today, no commercial CO_2 electroconversion routes are applied and we therefore base our process analysis on a (potential) demonstration facility. This plant at full load (8760 h/yr of operation) has an input capacity of around 1.0 ktCO_2 per year (Figure S1). This scale does approximately match the current development status of our key technology units but not the size of current fossil-based plants that produce for instance syngas or ethylene, which typically deal with feedstock flows that are three orders of magnitude larger (~1000 kt per year) (Petrochemicals Europe, 2022).[1] To accommodate for this mismatch between our six routes and industrial facilities, we assume that scale-up occurs during the development towards TRL 9 and that cost reduction in response to economies-of-scale is an intrinsic element of our technology learning curve. Both the state-of-the-art and the expected rates of development and system scale-up are discussed for each of the key technologies.

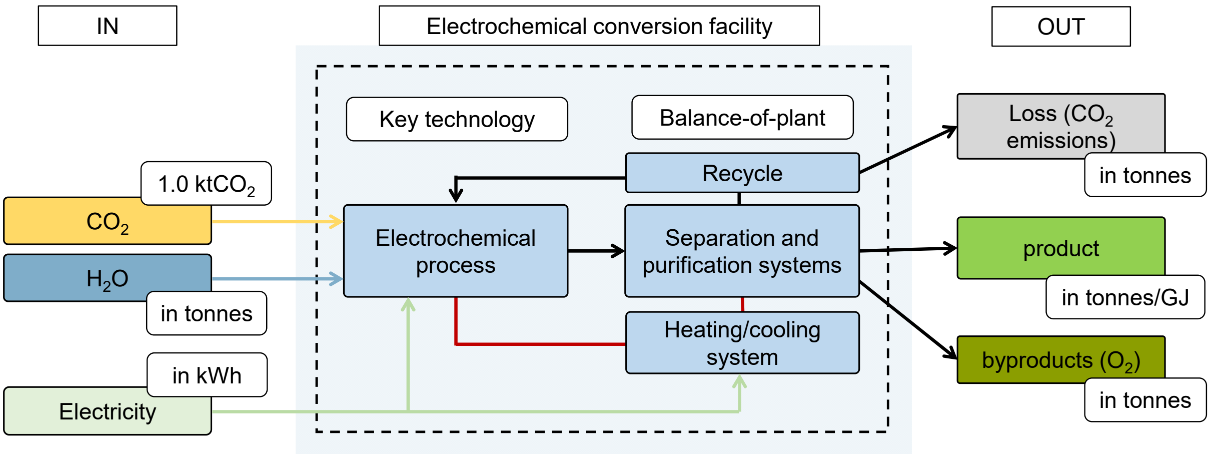

Figure S1. Schematic representation of a CO_2 electrochemical conversion route showing the system boundary (dashed box) and in- and outputs. Upstream CO_2 separation and purification steps are out-of-scope.

1.2 Energy and mass balances

The basic configuration as shown in Figure 1 indicates three different input streams: CO_2, H_2O, and electricity. If heat or steam is required, we assume it will be provided by an electric heating system, which operates at an efficiency of 95%. For each of the key technologies the stack efficiency is determined by dividing the energy of the desired product (in lower heating value (LHV)) by the electricity consumption of the key technology unit. The total energy efficiency of the route also includes the electricity used for balance-of-plant operation, such as electric heating, powering pumps, and energy use in buildings.

The conversion efficiency of the process is based on carbon in which we divide the amount of carbon in the product by the total amount of carbon in the CO_2 inlet stream (both in moles). Process selectivity, single pass conversion rates, and separation and recycling efficiencies together determine the losses and byproducts of the route. The portion of carbon that is not converted into the product and cannot be recycled results in a loss category, which includes for instance purge streams that are flared or vented and can result in CO_2 emissions, but also undesirable side products due to poor reaction selectivity. The byproducts category consists of compounds that are formed along with the desired product and cannot be avoided, e.g. oxygen. No value is attributed to the losses and byproducts. As mentioned in the introduction section in the main paper, the source of CO_2 substantially contributes to the sustainability of the approach and the production costs of the different compounds. CO_2 input is considered to be supplied from a circular source, such as from biogenic point sources, waste streams, or direct air capture (DAC). The costs of these sources may vary significantly and we explore their impact in a sensitivity analysis (Table S1).

The energy source to drive the electrochemical CO_2 conversion process is electricity. The origin of this electricity determines largely the sustainability and environmental impact of the routes. Many aspects of the conversion route do rely on assumptions regarding the electricity source, such as the costs of the electricity, the intermittency and amount of full load hours (FLH) of electricity supply, and the CO_2 emission factor of the electricity. To illustrate the dependence on the electricity source, we investigate the electricity costs and amount of FLH in a sensitivity analysis (Table S1). In Section 1.6, we describe how the environmental greenhouse gas (GHG) performance of the different routes were assessed.

1.3 Investment costs

The electrochemical conversion facility consists of the core technology unit, for instance a low temperature electrolyser, and the balance-of-plant equipment, such as the purification and heating/cooling systems. The total investment costs (CAPEX) are estimated for a 1.0 ktCO_2/yr plant and expressed in €(2020) (Table S1). The core technology and balance-of-plant equipment costs are determined based on literature sources (see state-of-the-art chapter in the main paper) and expert judgement and sum up to the direct CAPEX. We apply an installation factor of 2 on top of the direct CAPEX to accommodate for indirect and owners costs, such as for construction, design, engineering, buildings, permits, contingency, etc. (Hydrohub, 2022). Direct and indirect CAPEX combined result in the total installed CAPEX of our plant design. The operating and maintenance (O&M) costs (excl. electricity and CO_2 input) are set at 4% of the total installed CAPEX (typical between 2 and 5% as, e.g., described in Agora (2018) and Detz, *et al.* (2018)).[2,3] Total replacement costs of key technology components are calculated for each of the routes separately, annualized over the total plant lifetime, and added to the O&M costs.

1.4 Production costs

The levelized production costs (C_x) are calculated with equation (1) in which the total annual costs are divided by the amount of product generated annually (P_x) (Blok & Nieuwlaar, 2016).[4] The discounted annualized CAPEX (with α being the capital recovery factor), the annual O&M costs (including equipment replacement costs), and the annual feedstock costs F (for CO_2, electricity and water) represent the total annual costs. The capital recovery factor (α) is determined by equation (2) and is a function of the discount rate (r) and the plant lifetime (n). We here use a typical discount rate of 10% and a plant lifetime of 20 years (based on IEA (2020); Detz, *et al.* (2018))[3,5] and vary these values in the sensitivity analysis. We assume that the operational capacity of the plant in FLH is steady over the plant lifetime. For our base case, the FLH amount to

$$C_{\mathrm{x}} = \frac{\alpha \times \mathrm{CAPEX} + \mathrm{O\&M} + \mathrm{F}}{P_{\mathrm{x}}} \tag{1}$$

$$\alpha = \frac{r}{1 - (1 + r)^{-n}} \tag{2}$$

4000, which is based on intermittent renewable electricity supply (e.g. from offshore wind, or a combination of solar and wind parcs), while we explore a range of 2000 to 8000 FLH in the sensitivity analysis. We investigate an electricity cost range of 20 to 60 €/MWh of which 40 €/MWh is our base case value (IEA, 2020).[5] The costs of CO_2 as a feedstock may, depending on the source, vary significantly. Capture of biogenic CO_2 at industrial fermentation processes can provide CO_2 for around 10 €/ton (IEAGHG, 2021a),[6] while direct air capture technology, although currently still expensive, may in the future supply CO_2 for approximately 100-250 €/ton (Keith *et al*., 2018).[7] We apply for our base case a CO_2 feedstock cost of 50 €/ton, while a broader range (20-150 €/ton) is explored in the sensitivity analysis (Table S1). Water is supplied at 1 €/ton (Agora (2018)).[2] Costs are reported in €(2020), unless otherwise noted. Other currencies are converted to € in the year under consideration, and subsequently corrected for inflation by converting them to our reference year (2020).

Table S1. Parameters for analysis of CO_2 electroconversion routes

Parameter	Selected base value	Sensitivity range	Unit
Production capacity	1	1 - 100	ktCO_2 input/yr
Plant lifetime	20	15 - 25	years
Annual operating time	4000	2000 - 8000	h/yr
Discount rate	10	5 - 15	%
Euro Reference year	2020		
O&M cost factor	4	2 - 6	% of initial CAPEX
H_2O	1.0	0.5 – 2.0	€/tH_2O
CO_2	50	20 - 150	€/tCO_2
Electricity	40	20 - 60	€/MWh_e

1.5 Cost projections through learning curve analysis

Estimates of today's production costs of our six routes are substantially higher compared to those of conventional processes that generate the same products from fossil resources. The costs of these novel technologies are likely to decline significantly thanks to for instance scale-up, innovation, and learning-by-doing. These overall decline in costs of these phenomena together can be aggregated into a technology learning curve. A technology learning curve provides information on how fast costs (or another metric) decline in relation to the cumulative installed capacity (McDonald & Schrattenholzer, 2001; Ferioli *et al*., 2009).[8,9] Plotting empirical data of costs versus the cumulative installed capacity on two logaritmic axes generally results in a declining straight line. The slope of this line relates to the learning rate (LR), which specifies the rate (as a percentage) of cost reduction for each doubling in cumulative installed capacity. This relationship can be expressed by equation (3) in which C_{Xt} represents the costs for a cumulative installed capacity X_t, C_{X0} the initial costs at the initial cumulative installed capacity X_0, and b is the learning parameter from which the LR can be derived via equation (4).

$$C_{X_t} = C_{X_0}\left(\frac{X_t}{X_0}\right)^{-b} \quad (3)$$

$$LR = 1 - 2^{-b} \quad (4)$$

Many technologies, during their deployment, rather steadily follow their learning curve for many decades. Extrapolation of the historical learning curve can, thus, be a valuable tool to estimate future costs of a technology. For novel technologies a learning curve is generally non-existing or is not (yet) determined because barely any cumulative capacity has been installed and cost data is difficult to find. For such a technology, a learning curve can be estimated based on the state-of-the-art and an assumed learning rate. A learning curve (or data) of comparable technologies might provide a good starting point for such assumptions.

We apply learning curve analysis to the direct investment costs of the technologies in our routes. We extrapolate historical learning curves of these technologies or, if no data is available, of comparable technologies to project the cost curves up to at least 2030 for different compound annual growth rates (CAGRs) for the analyzed technologies. We apply a low and high CAGR to explore a range in cumulative installed capacity in 2030. The CAGR values are based on various reported scenarios and existing plans and announcements for (comparable) technology deployment. We do not consider any limitations regarding annual capacity additions due to restrictions in market size of a specific product category because we foresee that until 2030 the share of electrochemical CO_2 conversion capacity remains relatively low compared to conventional capacity. Most of our core technologies are mainly developed for hydrogen or electricity production, i.e. water electrolysers and solid oxide fuel cells. We postulate that the share of total capacity applied for electrochemical CO_2 conversion is relatively small in 2030. The specific amount of capacity employed for electrochemical CO_2 conversion cannot be deduced from the learning curves but will be discussed separately for each of the routes. We employ our CAPEX learning curves to calculate the future total investment costs (including indirect costs) and levelized production costs. We also project costs up to 2050. Although less reliable due to the many uncertainties regarding the successful scale-up of the conversion routes, such projections illustrate the possible trajectories of technology deployment and related cost reductions.

1.6 Environmental greenhouse gas performance

The sustainability of novel routes to convert CO_2 into various products is determined by their environmental impact over the total value chain. More detailed insight on several impact categories, such as climate change, ozone depletion, acidification, water use, and toxicity, requires extensive life-cycle analysis and is not the focus of this study. Here, we perform an analysis on the CO_2 emissions associated to each route to generate 1 GJ of product based on the emission factor of the electricity supply. The CO_2 feedstock is considered sustainable (i.e. originating from atmosphere, either directly via DAC or via biomass) and does not contribute to net emissions, not even when CO_2 is emitted again during the process via combustion of side products.

For each electrochemical route, we investigate the impact of the emission factor of electricity supply. We explore various levels of a decarbonized electricity: from 0-500 gCO2e/kWh and indicate the average grid emission factor in several regions in the world. The carbon intensity of the electrochemical processes is compared with the fossil reference (including end-of-life emissions) in terms of carbon footprint.

2 Supplementary state-of-the-art information

2.1 Chlor-alkali process

The schematics of the electrolysis cells for both the H_2 co-production and the oxygen depolarised cathode (ODC) system are given in Figure S2. The main particularity of the ODC system is the feeding of a gaseous O_2 stream to the cathode, and the suppression of the hydrogen evolution reaction (HER). The final products of the electrolysis from the ODC system are as well C_{l2} and a concentrated NaOH solution.

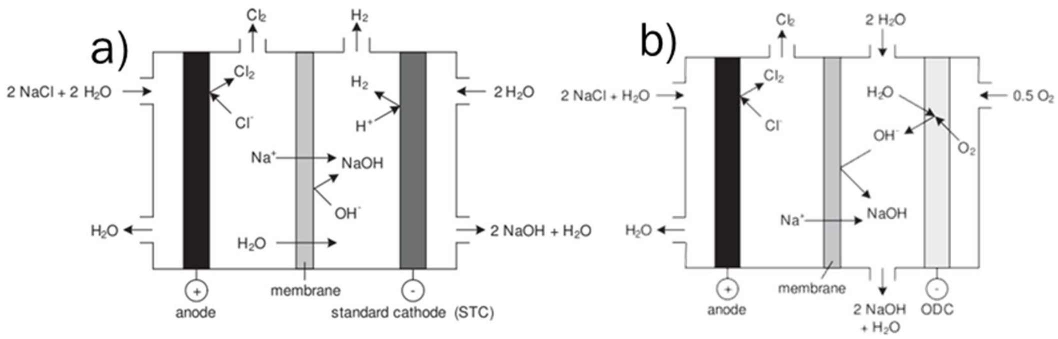

Figure S2. Schematic design and operation of a single electrolysis cell a) with H_2 co-production and ;b) with an Oxygen Depolarised Cathode (ODC), with coupled O_2 consumption (reproduced from Jung *et al.*, 2014).[10]

The complete mass and energy balances of both the H_2 co-production system and the ODC system for the chlor-alkali process are found in Table S2. The final purity of the Cl_2 gas is taken to be 98 vol%, according to Thyssenkrupp (2015).[11]

Table S2. Complete mass and energy balances for the chlor-alkali process, for H_2 co-production (H_2 co-p), and the Oxygen Depolarised Cathode (ODC) systems, based on the production of 1 kg Cl_2. Data retrieved from Jung *et al.*, 2014 and Eurochlor, 2018.[10,12]

Flow		**Unit**	**H_2 co-p**		**ODC**	
			Input	Output	Input	Output
Electricity	Stack	kWh_{el}	2.40	-	1.75	-
	Post-treatment	kWh_{el}	0.08-2.03	-	0.08-2.03	-
	Total	kWh_{el}	2.49-4.52	-	1.83-3.87	-
H_2O		kg	1.65-1.75	-	1.65-1.75	-
NaCl		kg	1.63-1.70	-	1.63-1.70	-
O_2		kg	-	-	0.25	-
Cl_2 (>98%vol)		kg	-	1	-	1
H_2 (>99,9%vol.)		kg	-	0.03	-	-
NaOH (aq. 32%wt.)		kg	-	1.13	-	1.13
NaOH (aq. 50%wt.)		kg	-	2.25	-	2.25

2.2 Route 1: Low-temperature CO_2 electroconversion to carbon monoxide

The complete mass and energy balances for the LT electrolysis of CO_2 to CO process is shown in Table S3.

Table S3. Complete mass and energy balances for the LT electrochemical reduction of CO_2 to CO. The category *'Aux.+DSP'* corresponds to the energy requirements of the PSA unit for CO purification (data from Jouny *et al*., 2018)[13] and the calcium caustic recovery loop for the CO_2 recovery in the anode side (data from Keith *et al*., 2018).[7] CO_2 emissions would correspond to the CO_2 content in the reject stream from the PSA unit.

Flow		Unit	**LT-CO**	
			Input	**Output**
Electricity	Stack	kWh_{el}	5.68-5.98	-
	Aux.+DSP	kWh_{el}	1.29-1.36	-
	Total	kWh_{el}	6.97-7.33	-
CO_2		kg	1.60-1.69	-
H_2O		kg	0.01	-
CO (98%vol.)		kg	-	1
O_2		kg	-	0.58-0.61
CO_2 emissions		kg	-	0.00-0.05
H_2		kg	-	0.00

Given the different power density for the water PEM electrolysis and the LT CO_2 electrolysis, the reported values for investment costs for the PEM systems are adapted to the performance indicators for LT CO_2 electrolysis. This can be done with the following equation (*5*), using the power density for both water PEM electrolysis and LT CO_2 electrolysis, as indicated by Barecka et al. (2021)[14]:

$$CAPEX(LT-CO_2)\left[\frac{€}{kW_{LT-CO_2}}\right] = CAPEX(PEM)\left[\frac{€}{kW_{PEM}}\right]\cdot\frac{PD(PEM)\left[{kW_{PEM}}/{m^2}\right]}{PD(LT-CO_2)\left[{kW_{LT-CO_2}}/{m^2}\right]} \quad (5)$$

2.3 Route 2: Low-temperature CO_2 electroconversion to formic acid

The simplified process flow diagram of the purification section of the electrochemical formic acid production process is depicted in Figure S3.

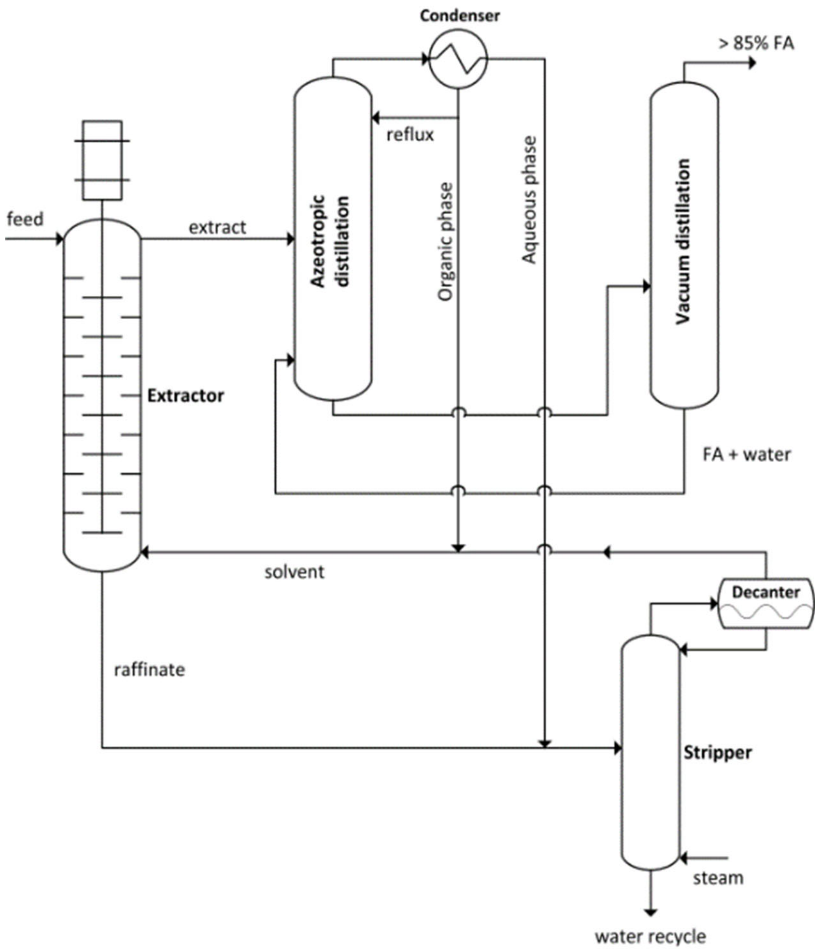

Figure S3. Hybrid extraction + azeotropic distillation strategy for the purification of an aqueous FA solution with a low boiling solvent. In the extractor, this solvent removes FA from water. The extract is sent to an azeotropic distillation column, recovering the azeotrope water-solvent at the top, and a highly concentrated FA stream at the bottom. The top fraction, biphasic, is split into two phases, being the organic phase (rich in solvent) partly recycled back to the azeotropic distillation column, and the rest being sent to a stripper to remove all water, along with the aqueous phase of the azeotropic distillation column. The bottom of this column is sent to a vacuum distillation column, in which an 85%wt. FA solution is recovered at the top. Reproduced from Ramdin *et al*., 2019.[15]

The complete mass and energy balances for the LT electrolysis of CO_2 to an aq. 85 wt% FA solution process is shown in Table S4.

Table S4. Complete mass and energy balances for the LT electrochemical reduction of CO_2 to FA. The category '*Aux.+DSP*' corresponds to the energy requirements of the hybrid extraction and azeotropic distillation for the purification of an aqueous FA stream up to 85 wt% (data from Ramdin *et al*., 2019).[15]

Flow		**Unit**	**LT-FA**	
			Input	**Output**
Electricity	Stack	kWh_{el}	4.08 – 5.09	-
	Aux.+DSP	kWh_{el}	1.42	-
	Total	kWh_{el}	5.50 – 6.51	-
CO_2		kg	0.81	-
H_2O		kg	0.58 – 0.79	-
FA (85%wt. aq.)		kg	-	1

Flow	Unit	LT-FA	
		Input	Output
O_2	kg	-	0.33 – 0.41
CO_2 emissions	kg	-	-
H_2	kg	-	0.00 – 0.01

2.4 Route 3: Low-temperature CO_2 electroconversion to ethylene

The complete mass and energy balances for the LT electrolysis of CO_2 to C_2H_4 process is shown in Table S5.

Table S5. Complete mass and energy balances for the LT electrochemical reduction of CO_2 to C_2H_4. The category *'Aux.+DSP'* corresponds to the energy requirements of the PSA unit for C_2H_4 purification (data from Jouny *et al.*, 2018a) and the calcium caustic recovery loop for the CO_2 recovery in the anode side (data from Keith *et al.*, 2018). CO_2 emissions would correspond to the CO_2 content in the reject stream from the PSA unit.

Flow		Unit	LT-C_2H_4	
			Input	Output
Electricity	Stack	kWh_{el}	75.7 – 79.7	-
	Aux.+DSP	kWh_{el}	2.89 – 3.05	-
	Total	kWh_{el}	78.6 – 82.7	-
CO_2		kg	4.62 – 4.78	-
H_2O		kg	2.85 – 2.92	-
C_2H_4 (99.9%wt.)		kg	-	1
O_2		kg	-	5.36 – 5.55
CO_2 emissions		kg	-	0.00 – 0.05
CO (side product)		kg		0.94
H_2		kg	-	0.17

2.5 Route 4: High-temperature CO_2 electroconversion to CO

Table S6 shows the overall mass and energy balance for the CO_2-SOE CO production route.

Table S6. Complete mass and energy balance for the CO_2- SOE to CO production.

Flow		Unit		
			Input	Output
Flow		Unit		
			Input	Output
Electricity	Stack	kWh_{el}	2.6 – 2.8	-
	Balance of plant	kWh_{el}	2.1 - 3.5	-
	Total	kWh_{el}	4.7 – 6.3	-

Flow	Unit		
		Input	Output
CO_2	kg	1.57-1.65	-
H_2O	kg	-	-
CO	kg	-	1
O_2	kg		0.54 – 0.57
CO_2 emissions	kg	-	-
Heat	GJ	-	-

2.6 Route 5: High-temperature CO_2 electroconversion to syngas

The overall mass balance for syngas production is given in the Table S7.

Table S7. Complete mass and energy balance for the HT co-electrolysis process for syngas production.

Flow		**Unit**		
			Input	**Output**[1]
Electricity	Stack	kWh_el	7.87	-
	Balance of plant	kWh_{el}	1.04	-
	Total	kWh_{el}	8.91	-
CO_2		kg	1.36	-
H_2O		kg	1.16	-
Syngas (H_2/CO) (H_2:CO = 2:1)		kg	-	1
O_2				1.50
CO_2 emissions		kg	-	-
H_2		kg	-	
Heat		GJ	-	-

[1] Schreiber *et al*., 2020[16]

2.7 High-temperature CO_2 molten carbonate electroconversion

Molten Carbonate Electrolysis Cell (MCEC) is a high temperature electroconversion technology (600-900°C) able to produce carbon monoxide (CO) or syngas (CO/H_2) (Hu, 2016). MCEC operating concept is based on the reversible operation of Molten Carbonate Fuel Cell (MCFC) technology, where the direction of the redox reactions is inversed (Figure S4). CO and syngas can respectively be produced by electrochemical conversion in a molten carbonate salt electrolyte (CO_3^{2-}) by feeding CO_2 or a mixture of steam and CO_2 streams at the fuel electrode (Monforti Ferrario *et al*., 2021).[17]

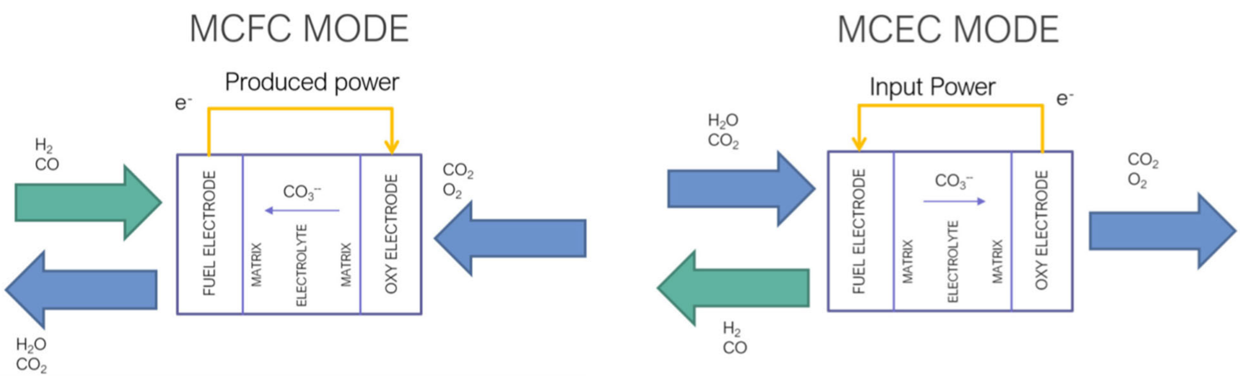

Figure S4. Scheme of the two operation modes of a Molten Carbonate Cells (MCC): (Right) MCC in the electrolysis (MCEC) mode and (Left) MCC in the FC (MCFC) mode (Monforti Ferrario *et al*., 2021).17

The MCEC technology has seen an increase of its development in the last few years, demonstrating the feasibility of both CO and syngas production processes at the lab-scale level (TRL 2-3), with experiments using button cells (Kaplan *et al*., 2010; Kaplan *et al*., 2014),[18,19] planar single cells (Hu, 2016; Hu *et al*., 2014; Meskine *et al*., 2021),[20,21,22] and numerical models (Perez-Trujillo *et al*., 2018; Perez-Trujillo *et al*., 2020).[23,24] An overview of the MCEC operating conditions and performance are presented in Table S8.

Table S8. Overview of MCEC systems properties for CO and syngas production.

	Unit	CO production[1]	Syngas production[2]
Fuel electrode reactions		$2CO_2 + 2e^- \rightarrow CO_2^{3-} + CO$	$H_2O + CO_2 + 2e- \rightarrow CO_3^{2-} + H_2$ $CO_2 + H_2 \leftrightarrow H_2O + CO$ (RWGS)
Oxygen electrode reactions		$CO_2^{3-} \rightarrow CO_2 + 1/2\ O_2 + 2e^-$	$CO_2^{3-} \rightarrow CO_2 + 1/2\ O_2 + 2e^-$
Operating temperature	°C	900	600-680°C
Current density	A/m^2	1000	1000 – 1600
Cell voltage	V	0.87	1.15 - 1.4
Faradaic efficiency	-	100%	100%
CO_2 utilisation degree	mole product/mole CO_2 in	85%	80%
Power density	kW/m^2	0.87	1.12 – 2.24

[1] Based on: Kaplan *et al*., 2010[18]; Kaplan *et al*., 2014[19]; Küngas, 2020[25]. [2] Based on: Monforti Ferrario *et al*., 2021[17]; Kaplan *et al*., 2010[18]; Kaplan *et al*., 2014[19].

The MCEC concept used for **syngas production** is based on the same system components as those used for the MCFC operating at in the temperature range of 600-680°C. In the reference studies on the topic (Hu, 2016; Monforti Ferrario *et al*., 2021; Kaplan *et al*., 2014),[21,17,19] the fuel electrode is made of porous nickel and/or alloyed with Cr and/or Al, the oxygen electrode of porous lithiated nickel oxide (NiO) and an electrolyte composed of a eutectic mixture of lithium, potassium, and/or sodium carbonate (Li_2CO_3, K_2CO_3, and Na_2CO_3), which remains liquid at the operating temperature (600-680°C). A porous matrix, commonly made of g-$LiAlO_2$, is used to retain the electrolyte, besides conducting the carbonate ions between the electrodes as well as separating the fuel and oxidant gases. A MCEC system based on this concept can operate at current density of 0.1 to 0.16 A/cm^2 for operating voltage between 1.15V and 1.4V, but the production of CO is rather limited (max 3%), about 30% of the CO_2 is converted to CH_4. (Monforti Ferrario *et al*., 2021).[17]

For **CO production**, the reversible MCFC technology based on Ni electrodes or Li-Na-K carbonate eutectic electrolytes was demonstrated to not be suitable under MCEC operations for this application (Kaplan *et al*., 2010; Kaplan *et al*., 2014).[18,19] The Ni fuel electrode used in MCFC systems was shown to coke almost instantaneously and a mixture of alkali metals subsequently intercalates the resulting surface graphite layer, leading to complete deactivation of the electrode. An alternative concept of MCEC technology for CO production, based on molten Li_2O/Li_2CO_3 electrolyte, a titanium fuel electrode and a graphite oxygen electrode has been shown to give promising results. The new concept operating at higher temperature (900°C) is able to deliver an efficiency of 85% at 0.1A/cm^2 for an operating voltage of 0.87V.

Regarding MCEC system integration, a system integration analysis at 1 MWe system scale has been carried out by Monforti Ferrario *et al.* (2021) in 2021 to integrate MCEC technology for the decarbonization of the reforming process of an oil refinery factory.[17] The integrated system design presented in Figure S5: Integrated system scheme and effects of the MCEC unit on a plant scheme (Monforti Ferrario *et al*., 2021).[17], aims to reuse 10-25% of the plant reformer off-gas in the MCEC stack, with intermediate gas processing with a PSA unit to achieve an equimolar H_2O:CO_2 ratio at the inlet of the MCEC stack needed for syngas production (Table S8). To optimize the efficiency of the system, a recycling of the off gas on the fuel outlet of the MCEC is aimed and the CO_2 stream outlet on the oxygen electrode side is also used for a process of Oxy-combustion integrated in the overall reforming process of the plant. With the MCEC stack integration with the following stack characteristics (650°C, 0.15 A/cm^2, 80% fuel utilization, 1 MWe, 490 m^2 cell area), several beneficial effects results for the operation of the refinery plant. The H_2 yield is increased by 3.06% with the recirculation of around 10% of the upgraded off-gas and an increase in the hydrogen yield up to 12% can be potentially achieved by increasing the installed power of the MCEC unit (4 MWe) to process the totality of the off-gas. The off-gas flow to the combustor is reduced by 7.93% at constant heat duty at the reformer combustor by increase of the integrated system efficiency (LHV of the upgraded off-gas). The MCEC integration also contribute to the reduction of CO_2 emissions with CO_2 reuse in the Oxy-combustion process. Last but not least, an electrochemical Specific Energy Consumption for the H_2 production of 3.24 kWh/Nm^3 H_2, which is a promising value in comparison with the competing low-temperature electrolysis technologies (between 5 and 6 kWh/Nm^3 H_2).

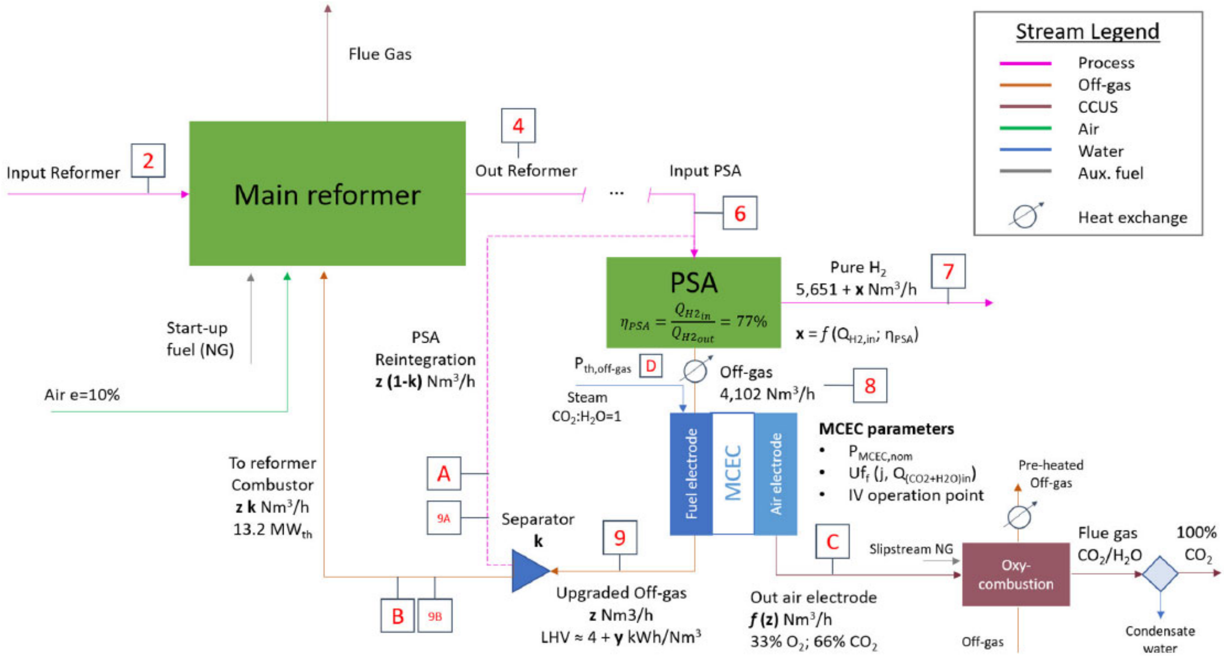

Figure S5: Integrated system scheme and effects of the MCEC unit on a plant scheme (Monforti Ferrario *et al*., 2021).[17]

Route 6: Tandem electroconversion approach to produce ethylene

Table S9. Complete mass and energy balances for the tandem route for the combination of HT CO production and LT CO conversion to C_2H_4. The energy requirements corresponding to the HT step (*'HT'*), both for the stack and for the auxiliaries, are referred to the production of 1 final kg C_2H_4. The category *'CO (HT intermediate)'* is the final CO stream coming from the HT step as input for the LT step. The category *'Aux.+DSP LT'* corresponds to the energy requirements of the PSA unit for C_2H_4 purification (data from Jouny *et al*., 2018)[13]. *'CO_2 emissions (HT)'* would correspond to the CO_2 content in the reject stream from the PSA unit in the HT step. *'CO emissions (LT)'* would correspond to the CO content in the reject stream from the PSA unit in the LT step.

Flow		**Unit**	**Tandem HT-CO + LT-CO-C_2H_4**	
			Input	Output
Electricity	Stack HT	kWh_{el}	4.78 – 5.09	-
	Stack LT	kWh_{el}	51.1 – 53.8	-
	Aux.+DSP HT	kWh_{el}	3.91 – 6.48	-
	Aux.+DSP LT	kWh_{el}	0.51 – 0.54	-
	Total	kWh_{el}	60.3 – 65.9	-
CO_2 (HT)		kg	5.03 – 5.47	-
H_2O (LT)		kg	5.73 – 5.80	-
CO (HT intermediate)		kg	3.20 – 3.31	
C_2H_4 (99.9%wt.)		kg	-	1
O_2 (HT+LT)		kg	-	8.41 – 8.50
CO_2 emissions (HT)		kg	-	0.00 – 0.34
CO emissions (LT)		kg	-	0.00 – 0.05
H_2 (side product LT)		kg	-	0.37
EtOH (side product LT)		kg	-	0.99

2.8 Technology and material summary of the different routes

The different design aspects and materials used for each technology covered in the state-of-the-art chapter in the paper are summarised in Table S10.

Table S10. Compendium of the materials, catalysts and cell designs used for the different electrochemical routes covered in chapter **Error! Reference source not found.**. Disclaimer: CER: Chlorine Evolution Reaction; HER: Hydrogen Evolution Reaction; OER: Oxygen Evolution Reaction; Aq.: aqueous; DI: de-ionised water.

Route	Cell reactor design	Membrane/separator	Electrolyte	Cathode catalyst material	Anode catalyst material
Chlor-alkali (co-produced H_2)	MEA with electrode foams in close contact with membrane[26]	Cation Exchange Membrane for Na^+ crossover Double-layer: sulfonic acid-based layer + carboxylic acid-based layer[27]	***Anolyte***: concentrated brine (aq. NaCl solution); ***Catholyte***: concentrated aq. NaOH solution[27]	Low-carbon steel; Ni foams for HER[1]	IrO_2, RuO_2 for CER Dimensionally Stable Anode (DSA) [27]
Chlor-alkali (ODC)	Semi-MEA: DSA foam in contact with membrane; cathode GDE to reduce O[26]			Ag-based catalyst for ODC[27]	
LT CO	MEA cell with 2 GDEs and feeding at the back of the electrodes[25]	AEM Sustainion for anion crossover[25]	***Anolyte***: aq. solution (can be alkaline); ***Catholyte***: absent; a humidified gaseous CO_2 stream is fed at the back of the cathode	Ag-based catalyst[25]	IrO_2-based catalyst for OER[25]
LT FA	3-compartment cell with 2 membranes and GDEs[28]	AEM Sustainion (formate crossover) + CEM Nafion (for proton crossover)[28]	***Anolyte***: aq. solution (can be alkaline); ***Centre compartment electrolyte***: DI water taking up produced FA; ***Catholyte***: absent; a humidified gaseous CO_2 stream is fed at the back of the cathode	Sn-based catalysts[28]; Bi_2O_3-based catalysts[29]	IrO_2-based catalyst for OER[25]
LT C_2H_4	MEA cell with 2 GDEs and feeding at the back of the electrodes[30]	AEM Sustainion for anion crossover[30]	***Anolyte***: aq. solution (can be alkaline); ***Catholyte***: absent; a humidified gaseous CO_2 stream is fed at the back of the cathode	Cu-based catalysts[30];	IrO_2-based catalyst for OER[25]
HT CO	Cell with three layers(Cathode, electrolyte, Anode) and one compartment for CO2 and one compartment for Air[31]		Solid ceramic material such as yttria-stabilized zirconia (YSZ), scandia stabilized zirconia (ScSZ)[3]	Ni-YSZ cermet [25]	Perovskites materials based on lanthanides and transition metals, such as Sr-doped LaMnO3(LSM),Sr-doped La(Fe,Co)O3 (LSCF),Sr-doped SmCoO3 (SSC) [25]
HT syngas	Cell with three layers(Cathode, electrolyte, Anode) and one compartment for mixed stream of CO2 and steam and one compartment for Air[31]		Solid ceramic material such as yttria-stabilized zirconia (YSZ), scandia stabilized zirconia (ScSZ) [25]		Perovskites materials based on lanthanides and transition metals, such as Sr-doped LaMnO3(LSM),Sr-doped La(Fe,Co)O3 (LSCF),Sr-doped SmCoO3 (SSC) [25]
MC CO	Porous electrode immersed in a molten carbonate salt		Electrolyte composed of a eutectic mixture of lithium, potassium, and/or sodium carbonate(Li_2CO_3, K_2CO_3, and Na_2CO_3)	Porous nickel and/or alloyed with Cr and/or Al	Porous lithiated nickel oxide (NiO)
Tandem C_2H_4 (HT-step)	(same as HT-CO)				

Route	Cell reactor design	Membrane/separator	Electrolyte	Cathode catalyst material	Anode catalyst material
Tandem C_2H_4 (LT-step)	MEA cell with 2 GDEs and feeding at the back of the electrodes[32]	CEM Nafion (for Na^+ crossover)[32]	***Anolyte***: aq. solution (can be alkaline); ***Catholyte***: NaOH and other C2+ products are collected in the 'wept' electrolyte through the membrane; a humidified gaseous CO stream is fed at the back of the cathode[32]	Cu-based catalysts[13];	IrO_2-based catalyst for OER[25]

3 Sensitivity analysis results

To illustrate the dependence of the total production costs on a single parameter, we have performed a sensitivity analysis for each of the routes, starting from the 2020 base case scenario. In Figure S6 to S9, the sensitivity analysis for, respectively, route 2, 3, 5, and 6 is presented.

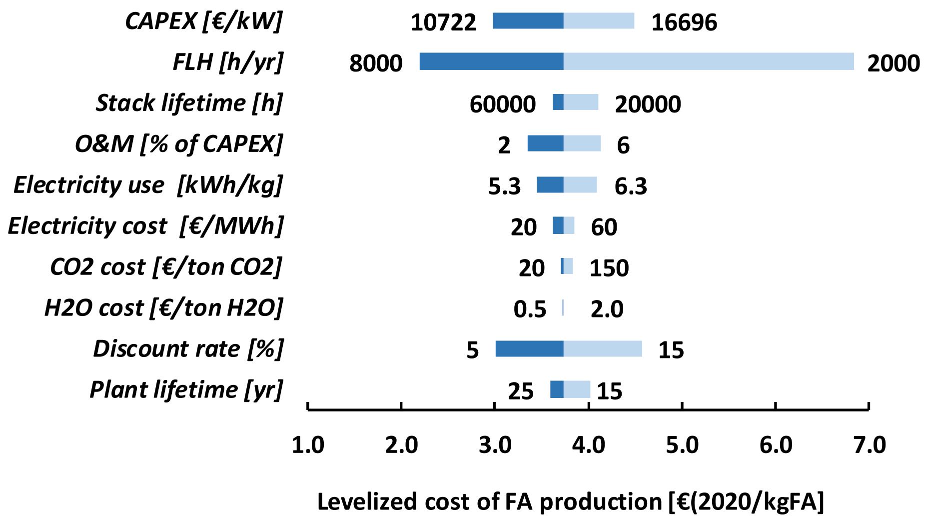

Figure S6. Sensitivity analysis for route 2 – LT electrochemical conversion of CO_2 to FA. Ten parameters are varied to explore their effect on the current levelized cost of formic acid production. The fossil reference formic acid price amounts to 0.70-0.80 €/kgFA.

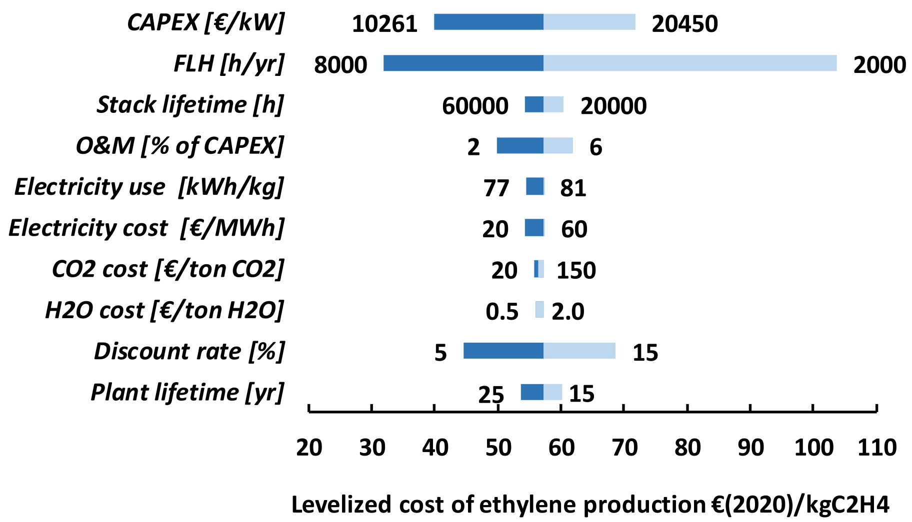

Figure S7. Sensitivity analysis for route 3 – LT electrochemical conversion of CO_2 to C_2H_4. Ten parameters are varied to explore their effect on the current levelized cost of ethylene production. The fossil reference ethylene price amounts to 0.70-1.30 €/kgC_2H_4

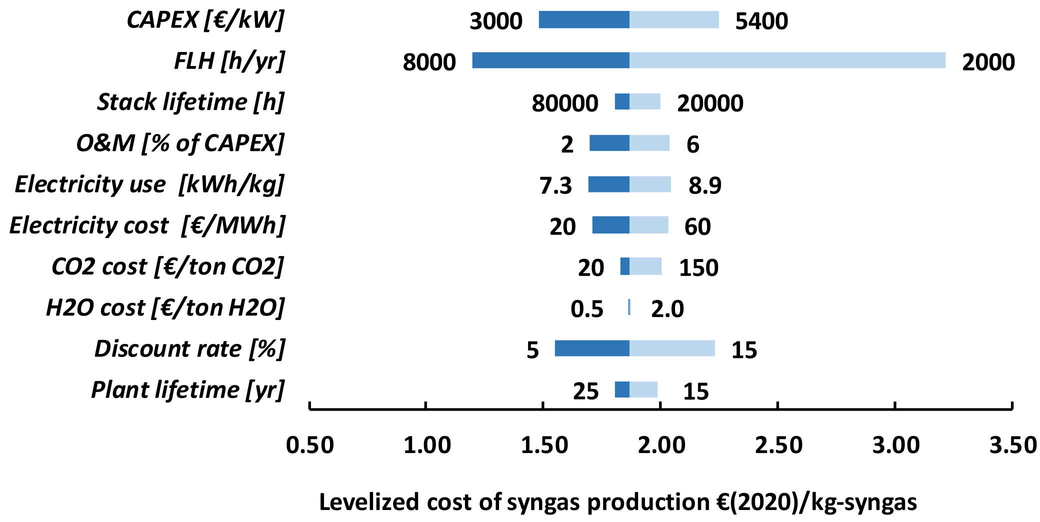

Figure S8. Sensitivity analysis for route 5 – HT electrochemical conversion of CO_2 to syngas. Ten parameters are varied to explore their effect on the current levelized cost of syngas production. The fossil reference syngas price amounts to 0.17-0.43 €/kg syngas.

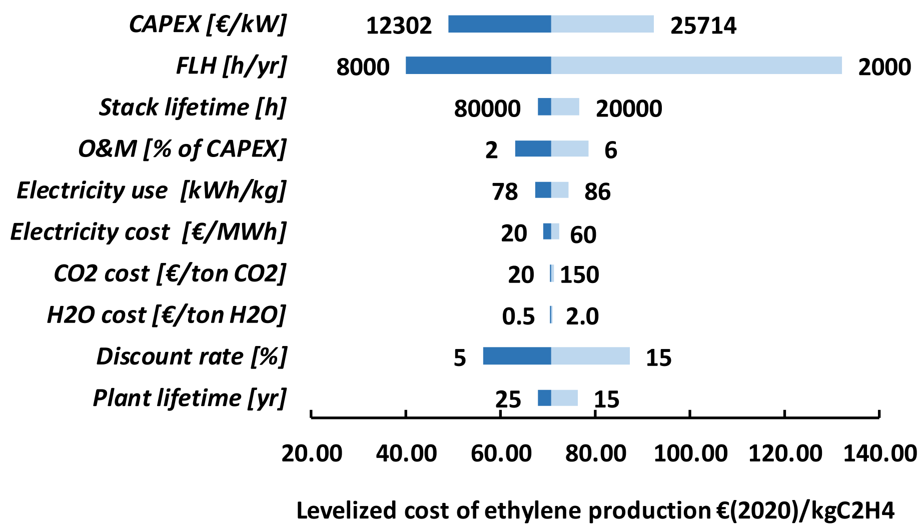

Figure S9. Sensitivity analysis for route 6 – Tandem HT/LT electrochemical conversion of CO_2 to C_2H_4. Ten parameters are varied to explore their effect on the current levelized cost of ethylene production. The fossil reference ethylene price amounts to 0.70-1.30 €/kgC_2H_4

4 References

[1] Petrochemicals Europe, 2022. Cracker capacity published on website. Retrieved from: https://www.petrochemistry.eu/about-petrochemistry/petrochemicals-facts-and-figures/cracker-capacity/

[2] Agora Verkehrswende, Agora Energiewende and Frontier Economics, 2018. The Future Cost of Electricity-Based Synthetic Fuels. Retrieved from: https://www.agora-energiewende.de/en/publications/the-future-cost-of-electricity-based-synthetic-fuels-1/

[3] R. J. Detz, J. N. H. Reek and B. C. C. van der Zwaan, *Energy & Environmental Science*, 2018, **11** (7), 1653 - 1669.

[4] K. Blok and E. Nieuwlaar, 2016. Introduction to Energy Analysis 2nd, Routledge, 2nd edn., 2016.

[5] International Energy Agency (IEA), 2020. Energy Technology Perspectives 2020. Special Report on Carbon Capture, Utilisation and Storage. Retrieved from: https://www.iea.org

[6] IEAGHG, 2021. CO_2 as a Feedstock: Comparison of CCU Pathways. IEAGHG Technical Report, 2021-02. Retrieved from: https://www.ieaghg.org/

[7] D. W. Keith, G. Holmes, D. St. Angelo and K. Heidel, *Joule*, 2018, **2** (8), 1573–1594. https://doi.org/10.1016/j.joule.2018.05.006

[8] A. McDonald and L. Schrattenholzer, *Energy Policy*, 2001, **29**, 255–261.

[9] F. Ferioli, K. Schoots, B. C. C. van der Zwaan, *Energy Policy*, 2009, **37**, 2525–2535.

[10] J. Jung, S. Postels and A. Bardow, *Journal of Cleaner Production*, 2014, **80**, 46–56. https://doi.org/10.1016/j.jclepro.2014.05.086

[11] Thyssenkrupp, 2015. Chlor-Alkali electrolysis plants. Superior membrane process. Retrieved from: http://www.thyssenkrupp-industrial-solutions-rus.com/assets/pdf/TKIS_Chlor-Alkali_Electrolysis.pdf

[12] Eurochlor, 2018. The Electrolysis process and the real costs of production. Retrieved from: https://www.eurochlor.org/wp-content/uploads/2019/04/12-electrolysis_production_costs.pdf

[13] M. Jouny, W. Luc and F. Jiao, *Industrial and Engineering Chemistry Research*, 2018, **57** (6), 2165–2177. https://doi.org/10.1021/acs.iecr.7b03514

[14] M. H. Barecka, J. W. Ager and A. A. Lapkin, *STAR Protocols*, 2021, **2** (4), 100889. https://doi.org/10.1016/j.xpro.2021.100889

[15] M. Ramdin, A. R. T. Morrison, M. De Groen, R. van Haperen, R. De Kler, E. Irtem, A. T. Laitinen, L. J. P. van den Broeke, T. Breugelmans, J. P. M. Trusler, W. de Jong and T. J. H. Vlugt, *Industrial and Engineering Chemistry Research*, 2019, **58** (51), 22718–22740. https://doi.org/10.1021/acs.iecr.9b03970

[16] A. Schreiber, A. Peschel, B. Hentschel, and P. Zapp, *Frontiers in Energy Research*, 2020, **8** (November), 1–17. https://doi.org/10.3389/fenrg.2020.533850

[17] A. Monforti Ferrario, F. Santoni, M. Della Pietra, M. Rossi, N. Piacente, G. Comodi and L. Simonetti, *Front. Energy Res.*, 2021, **9**, 655915., doi: 10.3389/fenrg.2021.655915

[18] V. Kaplan, E. Wachtel, K. Gartsman, Y. Feldman and I. Lubomirsky, *J. Electrochem. Soc.*, 2010, **157** B552

[19] V. Kaplan, E. Wachtel and I. Lubomirsky, *J. Electrochem. Soc.*, 2014, **161**, F54

[20] L. Hu, I. Rexed, G. Lindberg hand C. Lagergren, *International Journal of Hydrogen Energy*, 2014, **39** (23), 12323-12329

[21] L. Hu, 2016. Molten Carbonate Fuel Cells for Electrolysis, Doctoral Thesis of KTH Royal Institute of Technology, ISSN 1654-1081, ISBN 978-91-7595-928-3

[22] H. Meskine, E. Gurbuz, V. Albin, A. Melendez-Ceballos, M., Cassir, A. Ringuedé and V. Lair, *International Journal of Hydrogen Energy,* 2021, **46**, 14913-14921

[23] J. P. Perez-Trujillo, F. Elizalde-Blancas, S. J. McPhail, M. Della Pietra and B. Bosio, *Appl Energy*, 2020, **263,** 114630.

[24] J. P. Perez-Trujillo, F. Elizalde-Blancas, M. Della Pietra and S. J. McPhail, *Appl Energy*, 2018, **226**, 1037-1055.

[25] R. Küngas, *Journal of The Electrochemical Society*, 2020, **167** (4), 044508. https://doi.org/10.1149/1945-7111/ab7099

[26] Thyssenkrupp, 2022. Chlor-Alkali Solutions. Retrieved from: https://thyssenkrupp-nucera.com/chlor-alkali-solutions/

[27] K. Li, Q. Fan, H. Chuai, H. Liu, S. Zhang and X. Ma, *Transactions of Tianjin University*, 2021, **27** (3), 202–216. https://doi.org/10.1007/s12209-021-00285-9

[28] H. Yang, J. J. Kaczur, S. D. Sajjad and R. I. Masel, *Journal of CO_2 Utilization*, 2017, **20** (April), 208–217. https://doi.org/10.1016/j.jcou.2017.04.011

[29] H. Yang, J. J. Kaczur, S. D. Sajjad and R. I. Masel, *Journal of CO_2 Utilization*, 2020, **42** (October), 101349.

[30] C. M. Gabardo, C. P. O'Brien, J. P. Edwards, C. McCallum, Y. Xu, C. T. Dinh, J. Li, E. H. Sargent and D. Sinton, *Joule*, 2019, **3** (11), 2777–2791. https://doi.org/10.1016/j.joule.2019.07.021

[31] A. Hauch, R. Küngas, P. Blennow, A. B. Hansen, J. B. Hansen, B. V. Mathiesen and M. B. Mogensen, *Science*, 2020, **370** (186), eaba6118. doi: 10.1126/science.aba6118

[32] D. S. Ripatti, T. R. Veltman and M. W. Kanan, *Joule*, 2019, **3** (1), 240–256. https://doi.org/10.1016/j.joule.2018.10.007